Semiconductor Physics, Quantum Electronics & Optoelectronics, 2026. V. 29, No 1. P. 066-079.

Hetero- and low-dimensional structures

Charge-discharge processes in solid electrolyte heterostructures $Ag_{7-x}(Ge_{1-x}P_x)S_5I$ for electrochemical energy devices

V.S. Bilanych[1,2], A.A. Slyvka[1], S.I. Vorobiov[2], A.I. Pogodin[1], T.O. Malakhovska[1], I.M. Mohylyuk[1], V. Komanicky[2]

[1]*Uzhhorod National University, 46 Pidhirna Street, 88000 Uzhhorod, Ukraine*
[2]*Pavol Jozef Šafárik University, Park Angelinum 9, Košice 04001, Slovakia*
[*]*Corresponding author e-mail: vitaliy.bilanych@uzhnu.edu.ua*

Abstract. Charge-discharge processes in solid electrolyte heterostructures $Ag|Ag_{7-x}(Ge_{1-x}P_x)S_5I|Se$ with different Ge/P ratios were investigated. It was shown that heterovalent substitution of Ge^{4+} by P^{5+} in the argyrodite structure significantly affects the ionic conductivity, relaxation time, and polarization effects at the electrode–electrolyte interface. Using galvanostatic cycling and measuring current-voltage characteristics, the dependences of the parameters of $U(t)$ on the composition and cycle number were established. The diffusion coefficients, Ag^+ ion mobility, ionic resistance, and transference numbers were determined, confirming the predominantly ionic nature of charge transport ($t_{ion} \approx 0.994…0.999$). Comparison of the charging and discharging curves revealed an asymmetry of charge accumulation and release processes, associated with formation and decomposition of Ag_2Se phase as well as interfacial polarization. The obtained results demonstrate high ionic conductivity and stability of the compositions with partial substitution of Ge by P, indicating the promise of $Ag_{7-x}(Ge_{1-x}P_x)S_5I$ heterostructures for applications in solid-state electrochemical devices.

Keywords: superionic conductors, argyrodite structure, $Ag_{7-x}(Ge_{1-x}P_x)S_5I$, solid electrolyte heterostructures, Ag^+ ion diffusion, charge-discharge processes, interfacial polarization, solid-state electrochemical devices.

https://doi.org/10.15407/spqeo29.01.066
PACS 66.30.Dn, 66.30.H−, 81.05.Je, 81.05.Mh, 82.45.Yz, 84.60.Rb

Manuscript received 06.01.26; revised version received 05.03.26; accepted for publication 18.03.26; published online 25.03.26.

1. Introduction

Silver-based superionic conductors are particular among solid electrolytes due to their unique combination of high ionic conductivity, structural stability, and possibility of fine-tuning of their properties through isomorphic and heterovalent substitutions. Application of such conductors is considered in the field of solid-state electrochemical devices, ranging from low-power energy sources and sensors to prototypes of solid-state batteries and next-generation energy storage systems. Of particular interest are solid ionic conductors based on argyrodites of the type Ag_7MX_5Hal (M = Ge, Si, P; X = S, Se; Hal = Cl, Br, I), owing to their high ionic conductivity and potential for use in advanced electrochemical devices. These materials are characterized by a high degree of structural disorder in the Ag^+ cation sublattice. This disorder results in low activation energies for ionic transport and provides ionic conductivities $\sigma \sim 10^{-3}…10^{-2}$ S/cm at room temperature [1–6]. Such ionic conductivity values are comparable to or even higher than those of liquid electrolytes, opening prospects for developing solid-state batteries, sensors, and electrochemical cells with improved stability and safety.

Ag_7GeS_5I occupies an important place in this class of materials and is considered as a model compound for studying mechanisms of ionic charge transport. Its structure is characterized by partially occupied silver sites and a well-developed system of diffusion pathways [7]. The ionic mobility of Ag^+ in this compound is defined by the degree of structural disorder and the energy landscape, which makes it possible to finely adjust the transport properties through chemical modifications. One of the most effective modification methods is heterovalent substitution of Ge^{4+} by P^{5+}, leading to formation of solid solutions $Ag_{7-x}(Ge_{1-x}P_x)S_5I$ [8, 9]. Such substitution not only alters the local symmetry and volume of the silver migration channels but also affects the concentration of vacancies involved in transport. In this way, heterovalent defects are introduced and the configuration of the silver cation sublattice is modified. Such substitutions enable control over the degree of disorder, the concentration of vacancies, and the activation energy of ionic transport. As a result, significant changes in both the magnitude and the temperature dependence of ionic conductivity are observed, as demonstrated by a number of experimental and theoretical studies [8, 10, 11].

Measurements of frequency and temperature dependences of impedance in $Ag_{7-x}(Ge_{1-x}P_x)S_5I$ have shown that an increase in the phosphorus content can lead to enhanced ionic conductivity and reduced activation energy [8, 12] due to an increase of the density of free sites for Ag^+ migration as well as changes in the local symmetry and volume of conducting channels [8]. These effects are associated with enhancement of structural disorder and optimization of diffusion pathways for Ag^+ ions. Furthermore, phase transitions and structural rearrangements upon temperature variation were found to be directly linked to the peculiarities of silver transport in the argyrodite structure [10].

Studies using diffraction and spectroscopic methods confirmed correlation between the distribution of silver ions and the changes in the electrical properties upon doping [12]. Investigations of the electrical properties of $Ag_{7-x}(Ge_{1-x}P_x)S_5I$ solid solutions by impedance spectroscopy made it possible to separate the contributions of bulk conductivity, grain boundaries, and interfacial transitions [8,13]. It was shown that heterovalent substitution of Ge^{4+} by P^{5+} in $Ag_{7-x}(Ge_{1-x}P_x)S_5I$ causes non-monotonic dependence of the ionic conductivity on the composition. The highest ionic conductivity value, $\sigma_{ion} = 5.83 \cdot 10^{-2}$ S/cm (298 K), was obtained for $Ag_{6.75}(P_{0.25}Ge_{0.75})S_5I$ [14]. The lowest activation energy of transport, $E_a = 0.069$ eV, was recorded for $Ag_{6.5}(P_{0.5}Ge_{0.5})S_5I$ [14]. These values exceed the conductivity of the individual compounds Ag_6PS_5I and Ag_7GeS_5I, confirming the positive effect of heterovalent substitution.

Impedance spectroscopy revealed specific features of charge transport, showing that $Ag_{7-x}(Ge_{1-x}P_x)S_5I$ ceramics belong to mixed ionic-electronic conductors with $\sigma_{ion} >> \sigma_{el}$. Nyquist plots indicate presence of two types of boundaries, namely “sharp” grain boundaries with high resistance and “diffuse” boundaries and “bridges” between grains having lower resistance. Thus, the total conductivity is defined by both bulk ionic conduction and transport through the intergranular regions.

Comparison of ceramics obtained from microcrystalline and nanocrystalline powders showed that a decrease in the average crystallite size to ~100…160 nm in nanopowders was accompanied by an increase in ionic conductivity. Recrystallization led to formation of micro- and intergranular defects (microcracks, micropores), which affected the electrical parameters. Nevertheless, a stable increase in σ_{ion} compared to the initial microcrystalline powder-based samples was observed. For $Ag_{6.5}(P_{0.5}Ge_{0.5})S_5I$, the conductivity increased from $3.62 \cdot 10^{-2}$ to $3.84 \cdot 10^{-2}$ S/cm with decreasing the crystallite size as a result of recrystallization [13].

Overall, $Ag_{7-x}(Ge_{1-x}P_x)S_5I$ ceramics exhibit the conductivity values comparable to or even exceeding those of single-crystal Ag_6PS_5I and Ag_7GeS_5I. The greatest improvements in σ are associated with optimized compositions ($x \approx 0.25…0.5$) and reduced grain size while maintaining phase homogeneity [12–14]. It was found out as a result of these studies that: (i) the electrical properties of the $Ag_{7-x}(Ge_{1-x}P_x)S_5I$ strongly depend on its composition, which is related to changes in vacancy concentration and the degree of disorder in the Ag^+ sublattice; (ii) heterovalent substitution of Ge^{4+} by P^{5+} enables record-high ionic conductivities (up to $5.83 \cdot 10^{-2}$ S/cm at 298 K); (iii) microstructure plays a key role, namely reduced crystallite size and controlled recrystallization enhance ionic transport; (iv) ceramic samples have a potential for practical applications in solid-state electrochemical devices, since they combine high σ_{ion} with relative moisture stability [8, 12–14].

Therefore, superionic materials of $Ag_{7-x}(Ge_{1-x}P_x)S_5I$ family represent a promising platform for developing solid-state electrochemical cells. Their high ionic mobility, tunable by composition, together with compatibility with chalcogenide electrode materials (*e.g.*, Se and Ag_2Se), open new ways for designing energy-efficient devices with controlled charge-discharge processes, in particular solid-state electrochemical devices and energy storage systems. Fully solid-state electrochemical devices (SSEDs) can provide enhanced safety, a wide electrochemical stability window, and compact form factors compared to their liquid electrolyte counterparts [15–18]. Implementation of these advantages depends on solid electrolytes (SEs) that must combine high ionic conductivity at room temperature with good interfacial compatibility and processability.

In addition to charge transport, interfacial chemistry critically determines practical behavior of superionic elements. In chalcogenide electrodes, Ag^+ exchange may lead to formation of silver chalcogenides (*e.g.*, Ag_2Se) at buried interfaces, altering charge transfer kinetics, interfacial resistance, and cycling stability. Thermodynamic and electrochemical studies of Ag–Se systems consistently indicate formation of Ag_2Se under electrochemical driving forces, meaning that Ag|SE|Se cells serve as a useful model platform for studying coupled phenomena of ionic transport and interphase formation in Ag-ion-based elements [19–21]. Studies of solid-state galvanic and electromagnetic compatibility as well as recent investigations of thin films support this mechanistic picture.

Despite significant progress in the study of crystal chemistry and ionic conductivity of these materials, open questions regarding influence of structural defects, degree of heterogeneity, and mechanical stresses in polycrystalline samples on their electrical properties still remain. In particular, charge-discharge processes in electrochemical cells based on these solid electrolytes, as well as the effect of anode and cathode materials on the stability of interfacial boundaries, are still insufficiently explored.

In this work, we report on the charge-discharge behavior of a solid-state electrochemical cell fabricated using a superionic ceramic electrolyte $Ag_{7-x}(Ge_{1-x}P_x)S_5I$ and an intermediate selenium film serving as a cathode. Inclusion of the Se interlayer enables realization of a heterostructure that promotes efficient ionic conduction and a specific distribution of electric potential within the cell architecture. The study is aimed at understanding the

electrophysical properties of such superionic materials in electrochemical systems as well as identifying their behavior under current flow in a potentiostatic regime. Correlating composition with transport metrics and electrode polarization provides insights into how the Ge/P ratio influences Ag^+ conduction pathways and the dynamics of interfacial reactions, including the tendency to form Ag–Se interphase. Such findings are essential for designing silver-based solid-state electrochemical devices. These devices exploit argyrodite chemistry to balance high ionic conductivity with stable low-resistance interfaces, thereby advancing silver-based solid-state electrochemical technologies.

2. Experimental

2.1. Sample preparation

To fabricate heterostructures based on solid electrolytes $Ag_{7-x}(Ge_{1-x}P_x)S_5I$, the end members Ag_6PS_5I and Ag_7GeS_5I as well as their solid solutions with the compositions (x = 0.75, 0.5, 0.25), namely $Ag_{6.25}P_{0.75}Ge_{0.25}S_5I$, $Ag_{6.5}P_{0.5}Ge_{0.5}S_5I$, and $Ag_{6.75}P_{0.25}Ge_{0.75}S_5I$, were synthesized. Similarity of the lattice parameters of the Ag_6PS_5I and Ag_7GeS_5I [22–24] enables preparation of solid solutions on their basis. Initially, Ag_6PS_5I and Ag_7GeS_5I were synthesized in evacuated (to 0.13 Pa) quartz ampoules. The synthesis was carried out from elementary Ag (99.995%), P (99.99%), S (99.999%) and Ge (99.99%) and pre-synthesized AgI taken in stoichiometric ratios. The technological conditions for the synthesis of the solid solutions $Ag_{7-x}(Ge_{1-x}P_x)S_5I$ are described in [12, 23]. As a result, bulk solid solution samples of $Ag_{7-x}(Ge_{1-x}P_x)S_5I$ (x = 0.75, 0.5, 0.25) with a mass of about 20 g were obtained.

For preparing superionic ceramics, the synthesized materials were ground in an agate mortar and sieved through a 10 μm mesh. The obtained powders were pressed in disks 10 mm in diameter and 1 mm thick by cold pressing at 25 °C under a pressure of 400 MPa. To obtain ceramic materials, the pressed disks were annealed for 36 h at 650 °C in quartz ampoules evacuated to 0.13 Pa [12]. This treatment led to recrystallization of the micropowders of the respective composition and formation of a ceramic structure. The surfaces of the ceramic disks were subsequently polished. These disks were then used to fabricate electrochemical cells based on solid electrolytes from superionic ceramics $Ag_{7-x}(Ge_{1-x}P_x)S_5I$.

Silver was used as the anode, since silver ions are the charge carriers in the superionic ceramics $Ag_{7-x}(Ge_{1-x}P_x)S_5I$ [12]. For this purpose, silver paste was applied to one polished surface of the superionic solid electrolyte disks using a micropipette, forming a uniform layer with a thickness several tens of micrometers. After application, the samples were thermally treated at 120…150 °C for 20…30 min in air to remove the organic binder and to fix the silver layer. As a result, dense, adhesive silver electrodes with low contact resistance were formed on the disk surfaces, ensuring reliable electrical contact between the superionic material and the external measuring leads.

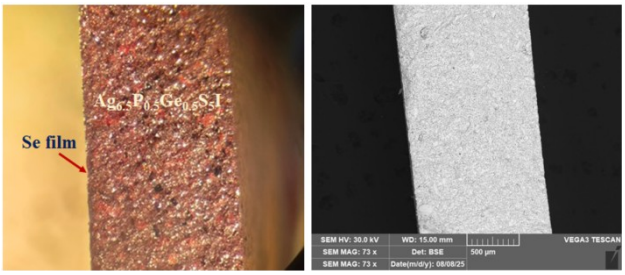

Fig. 1. Cross-sectional images (fractured surface) of the "Ag|SE|Se" structure based on $Ag_{6.5}P_{0.5}Ge_{0.5}S_5I$ ceramics obtained by (a) optical microscopy and (b) scanning electron microscopy (SEM).

A selenium film was used as the cathode. The selenium film was deposited by thermal evaporation in vacuum from ground vitreous selenium onto the second polished surface of the superionic solid electrolyte disks of $Ag_{7-x}(Ge_{1-x}P_x)S_5I$. The film thickness was measured on a witness sample (a selenium film on a transparent sapphire substrate deposited in the same cycle) by an interferometric method using a MII-4 interference microscope. The selenium film thickness was found to be 8.2 (±0.2) μm. Subsequently, a 50 nm thick gold layer was deposited on top of the selenium film by magnetron sputtering.

As a result, $Ag|Ag_{7-x}(Ge_{1-x}P_x)S_5I|Se$ ("Ag|SE|Se", where SE denotes the superionic electrolyte $Ag_{7-x}(Ge_{1-x}P_x)S_5I$) structures were fabricated. The cross-sectional images of such a structure are shown in Fig. 1.

To ensure reliable electrical connection of the electrochemical cells to the measuring equipment, current-collecting pads were formed on the Ag and Au film surfaces. Copper wires were used as leads and were attached to the metallic films with conductive silver adhesive, which provided stable electrical contact, ensured connection of the cell to a potentiostat, and minimized interfacial resistance.

The fabricated Ag|SE|Se electrochemical cells were used for measuring galvanostatic charge-discharge curves, studying compositional dependence of the characteristic parameters governing the charge-discharge behavior in the $Ge^{4+} \leftrightarrow P^{5+}$ substitutional series, and recording the current-voltage characteristics (CVC) of the Ag|SE|Se cells.

All the measurements were carried out in a two-electrode configuration at room temperature using an Autolab PGSTAT302F potentiostat/galvanostat (Metrohm Autolab B.V.). The experimental protocols were controlled by a Nova software. Galvanostatic cycling was performed under a constant current simultaneously recording the cell voltage as a function of time. The CVC were measured in potentiostatic mode under linear voltage sweep conditions. The obtained charge-discharge profiles and $I = f(V)$ curves were used to analyze the mechanisms of Ag^+ ion transport in the superionic electrolyte, to evaluate influence of the chemical composition ($Ge^{4+} \leftrightarrow P^{5+}$ substitution) on the reaction kinetics, and to determine the electrochemical characteristics of the investigated heterostructures.

3. Results and discussion

3.1. Structure and chemical composition of the Ag|SE|Se electrochemical cell

The real structure of the Ag|SE|Se cell was investigated using a TESCAN VEGA scanning electron microscope. The chemical composition and elemental distribution were analyzed by energy-dispersive X-ray spectroscopy (EDS). Figs 2a–2d show SEM images of the fractured surface of the superionic ceramic disk.

It can be seen that the ceramic microstructure is highly inhomogeneous, containing crystallites of various sizes and micropores formed during recrystallization. The structure exhibits both distinct grain boundaries with sharp interfaces and continuous "bridges" connecting neighboring crystallites. Figs 2c and 2d also demonstrate that the selenium film uniformly covers the polished ceramic surface, confirming formation of a hetero-junction across the entire surface of the superionic disk.

Elemental distribution maps and the chemical composition in the vicinity of the Se|SE heterostructure were obtained using energy-dispersive X-ray analysis (Figs 3 and 4). As can be seen from Fig. 3, the elemental distribution inside the crystallites and in the intercrystal-line regions is nearly identical. On the fresh fracture surface of the electrochemical cell, a small amount of silver was also detected in the selenium film at its interface with the superionic ceramic. This indicates that silver atoms diffused into the selenium film during storage of the electrochemical cells at room temperature under daylight exposure. It is well known that diffusion of Ag along thin Se films leads to formation of Ag_2Se crystallites [25–28]. As a result, a selenium layer with silver admixture is formed, exhibiting electronic conductivity. Consequently, a junction is created between pure selenium (*p*-type semiconductor) and selenium with silver admixture (*n*-type semiconductor), *i.e.*, a *p-n* junction is formed.

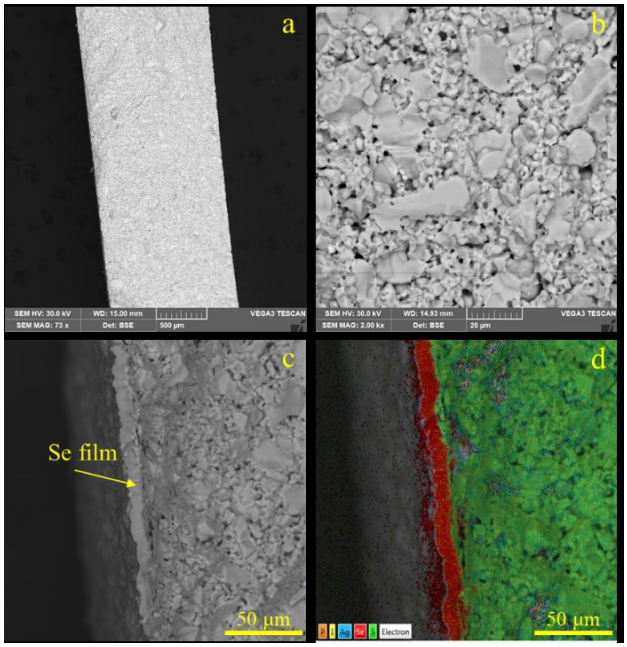

Fig. 2. Structure of the Ag|SE|Se cell: (*a*) SEM cross-sectional scan of the Se|SE|Ag heterostructure; (b) SEM image of the fresh fracture surface of $Ag_{6.5}P_{0.5}Ge_{0.5}S_5I$; (c) SEM image of the fresh fracture surface of the SE|Se heterostructure; (d) elemental distribution map near the SE|Se heterostructure.

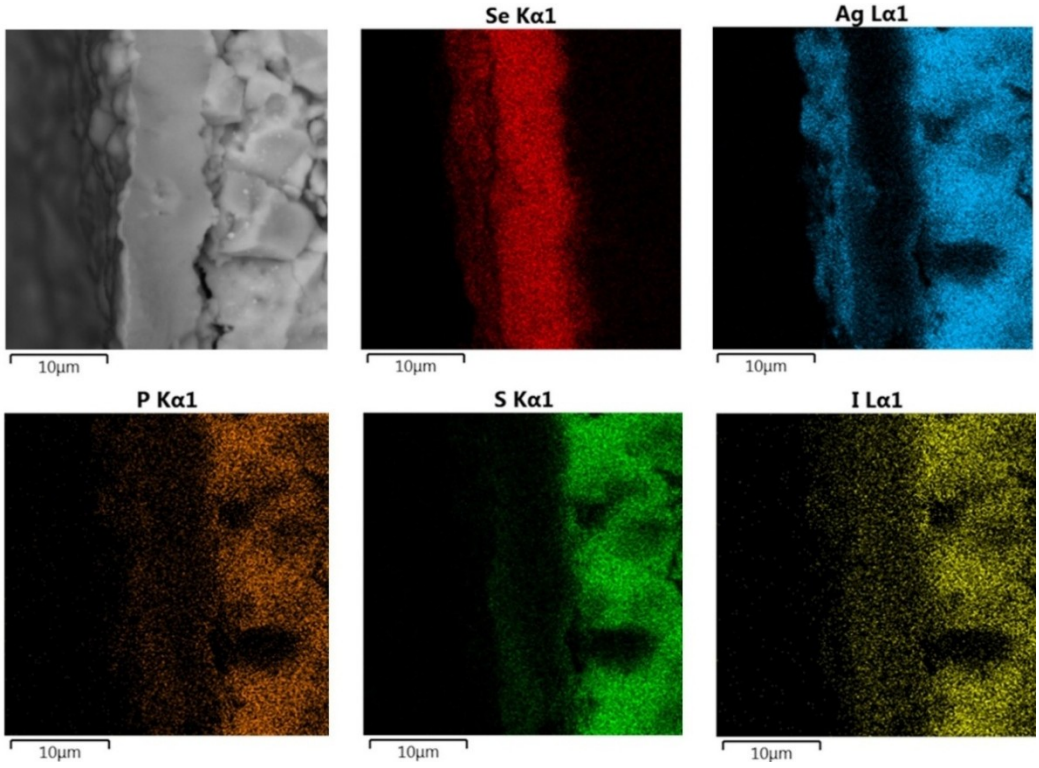

Fig. 3. Elemental distribution maps across the cross-section of the SE|Se heterostructure region.

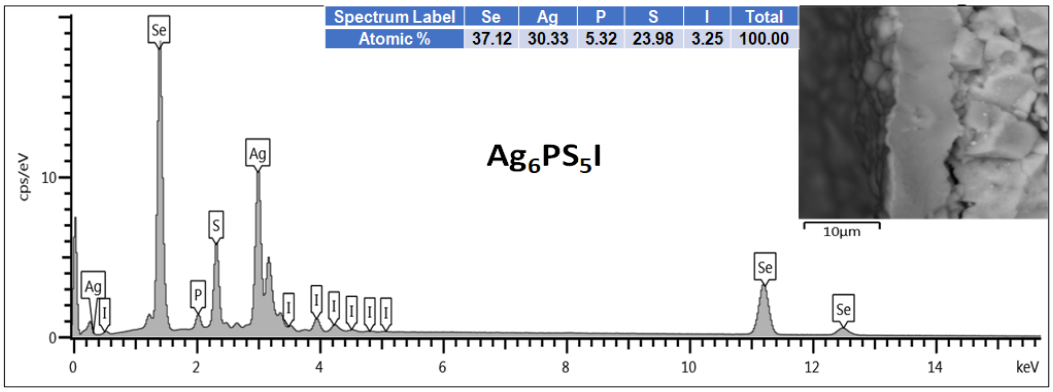

Fig. 4. Results of energy-dispersive X-ray analysis of the chemical composition in the vicinity of the Se|SE contact in the Ag_6PS_5I-based electrochemical cell.

3.2. Operation principle of the $Ag|Ag_{7-x}(Ge_{1-x}P_x)S_5I|Se$ electrochemical cell

In the investigated electrochemical cells, ionic conductivity and reversible electrochemical reactions occur at the interfaces. The silver electrode (Ag) acts as a source of ionically mobile component Ag^+. The solid electrolyte $Ag_{7-x}(Ge_{1-x}P_x)S_5I$ exhibits superionic conductivity due to the high mobility of silver ions in its crystal lattice. Its main function is to provide Ag^+ transport from the silver electrode to the opposite electrode. The selenium electrode (Se) serves as a cathode, where silver ions can be intercalated leading to formation of compounds of the Ag_2Se type.

During charging, a positive potential is applied to the silver electrode. Under this bias, silver atoms are oxidized:

$$Ag \rightarrow Ag^+ + e^- . \quad (1)$$

The Ag^+ ions migrate through the superionic electrolyte $Ag_{7-x}(Ge_{1-x}P_x)S_5I$ towards the Se cathode. At the SE|Se interface, they are reduced:

$$2Ag^+ + 2e^- + Se \rightarrow Ag_2Se . \quad (2)$$

As a result, Ag_2Se crystallites are formed at the SE|Se interface and within the selenium film [25].

During discharge, upon reversal of the external potential, the opposite process becomes thermodynamically favorable. The Ag_2Se phase decomposes:

$$Ag_2Se \rightarrow 2Ag^+ + 2e^- + Se . \quad (3)$$

The released Ag^+ ions migrate back into the solid electrolyte and diffuse toward the silver electrode, where they are reduced:

$$Ag^+ + e^- \rightarrow Ag . \quad (4)$$

Therefore, silver is redeposited at the anode, while the selenium electrode is released from the intercalated ions. The overall operation of the cell is governed by an entirely solid-state mechanism, in which Ag^+ ions migrate through the solid electrolyte, while electrons move through the external circuit. The key reversible process determining the charge-discharge characteristics is the formation and decomposition of Ag_2Se at the SE|Se interface.

3.3. Galvanostatic charge-discharge cycles

Cyclic measurements of voltage-time dependence $U(t)$ of the solid-state electrochemical cells based on superionic electrolytes $Ag_{7-x}(Ge_{1-x}P_x)S_5I$ with varying Ge/P ratios were carried out under a constant charge-discharge current of $I = 1$ mA. The experiments were performed using an AUTOLAB PGSTAT302N potentiostat/galvanostat. Fig. 5 presents the charge-discharge characteristics of the cells for five consecutive cycles. As can be seen from Fig. 5, the voltage monotonously increases with charging time, while its growth rate gradually decreases at longer times. Substitution of Ge^{4+} by P^{5+} leads to an increase in the voltage absolute values as well as changes in the slope of $U(t)$ during charging. The charging curves demonstrate a decelerating growth: during the first few minutes of charging (10 min in total), the voltage rises sharply and then gradually approaches a quasi-linear region with a weak slope. These linear segments are most clearly observed for the compositions $Ag_{6.75}P_{0.25}Ge_{0.75}S_5I$ and $Ag_{6.5}P_{0.5}Ge_{0.5}S_5I$. The evolution of the charge-discharge curves with cycling strongly depends on the Ge/P ratio. For the samples (a), (d), and (e), the rate of the voltage increase at the end of charging decreases with the cycle number. For the sample (b), the growth rate remains almost constant across all the cycles. In contrast, for the sample (c), the voltage rise becomes significantly faster at increasing the cycle number.

Analysis of the charging curves over five cycles shows that the experimental dependences $U(t)$ can be best approximated by a sum of exponential and linear functions as follows:

$$U(t) = \left(U_0 - A_0 e^{-t/\tau}\right) + \left(k \cdot t + b\right). \quad (5)$$

Here, U_0 is the limiting voltage approached at long charging times, A_0 is the amplitude of the exponential growth, τ is the characteristic relaxation time, k is the coefficient describing the linear voltage increase with time, associated with slow irreversible processes (polarization, charge accumulation at interfaces, or diffusion limitations), and b is the offset constant (initial value of the linear contribution at $t = 0$), respectively.

Table 1. Fitting parameters of the $U(t)$ dependences for the cells in the fifth charging cycle.

	Chemical composition	U_0, V	A_0, V	τ, s	k, V/s	b, V
1	Ag_7GeS_5I	0.212	0.175	27.1	$0.33\cdot10^{-5}$	0.203
2	$Ag_{6.75}P_{0.25}Ge_{0.75}S_5I$	0.315	0.236	32.6	$2.79\cdot10^{-5}$	0.318
3	$Ag_{6.5}P_{0.5}Ge_{0.5}S_5I$	0.317	0.168	40.4	$15.5\cdot10^{-5}$	0.320
4	$Ag_{6.25}P_{0.75}Ge_{0.25}S_5I$	0.36	0.072	67.7	$0.67\cdot10^{-5}$	0.359
5	Ag_6PS_5I	0.405	0.055	74.1	$0.60\cdot10^{-5}$	0.404

For a more accurate determination of the fitting parameters, each experimental dependence $U(t)$ was decomposed into its exponential and linear components. Fig. 6 presents the measured experimental curve together with its exponential and linear contributions for the $Ag_{6.5}P_{0.5}Ge_{0.5}S_5I$ cell.

In a similar manner, the dependences $U(t)$ were decomposed and approximated for other cycles and for various $Ag_{7-x}(Ge_{1-x}P_x)S_5I$ compositions. Table 1 summarizes the approximation parameters of the $U(t)$ dependences for all the cells in the fifth charging cycle. Fig. 7 presents the dependences of the approximation parameters of the charging curves $U(t)$ for the 5th charging cycle on the chemical composition of $Ag_{7-x}(Ge_{1-x}P_x)S_5I$.

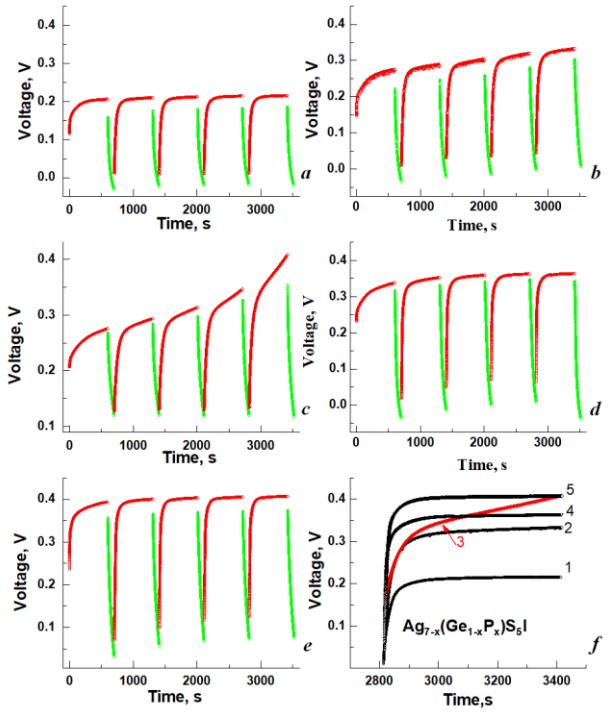

Fig. 5. Time dependence of the cell voltage during five charge-discharge cycles: a) Ag_7GeS_5I, b) $Ag_{6.75}P_{0.25}Ge_{0.75}S_5I$, c) $Ag_{6.5}P_{0.5}Ge_{0.5}S_5I$, d) $Ag_{6.25}P_{0.75}Ge_{0.25}S_5I$, e) $Ag_6P_5S_5I$, and f) voltage–time charging curves for the fifth cycle (*1* – Ag_7GeS_5I, *2* – $Ag_{6.75}P_{0.25}Ge_{0.75}S_5I$, *3* – $Ag_{6.5}P_{0.5}Ge_{0.5}S_5I$, *4* – $Ag_{6.25}P_{0.75}Ge_{0.25}S_5I$, and *5* – $Ag_6P_5S_5I$).

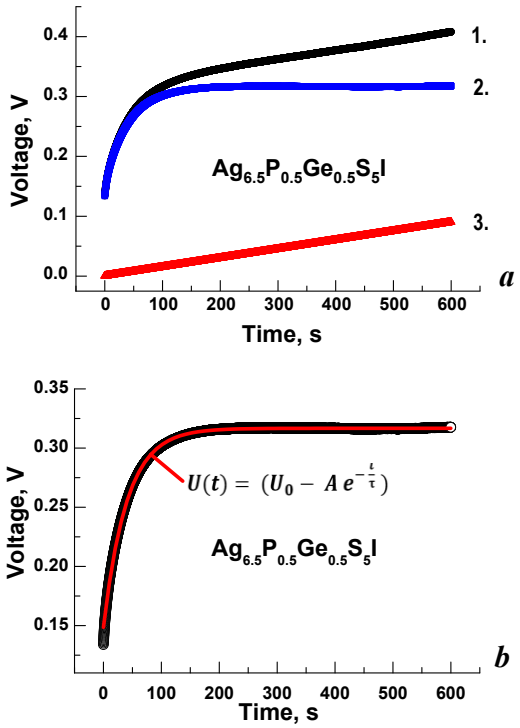

Fig. 6. Charging curves of the cell. a) Experimentally measured dependence $U(t)$ (*1*), together with its exponential (*2*) and linear (*3*) components for the $Ag_{6.5}P_{0.5}Ge_{0.5}S_5I$ cell. b) Results of the $U(t)$ curve fitting.

Approximation of the charging curves $U(t)$ by the sums of exponential and linear functions made it possible to separate the fast relaxation processes, characterized by the parameters A and τ, from the slow irreversible processes, which are reflected in the linear growth coefficient k. It can be seen from Fig. 7 that the approximation parameters systematically vary at increasing the phosphorus content in the $Ag_{7-x}(Ge_{1-x}P_x)S_5I$ ceramics. The limiting voltage U_0 increases from 0.212 V for Ag_7GeS_5I to 0.405 V for Ag_6PS_5I. This indicates an increase in the electromotive force of the cells upon substitution $Ge^{4+} \rightarrow P^{5+}$, which may be related to changes in the defect structure and ionic mobility [29]. The amplitude of the exponential component A_0 decreases with increasing the phosphorus content from 0.236 V at x = 0.25 to 0.055 V at x = 1.0. The decrease in A_0 suggests a reduction in the contribution of fast charge

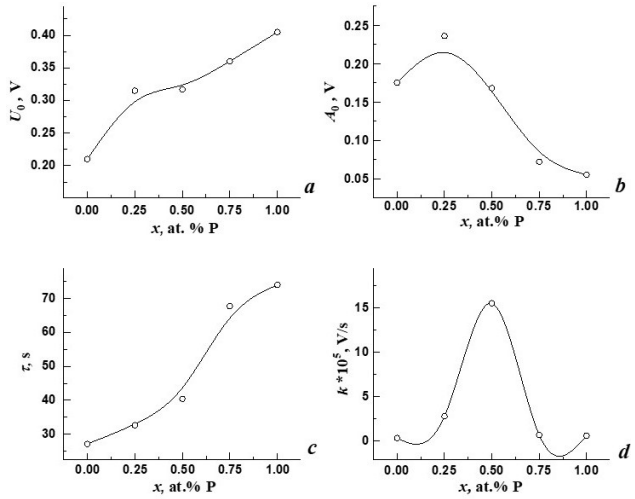

Fig. 7. Variation of the approximation parameters of the charging curves $U(t)$ with the chemical composition of $Ag_{7-x}(Ge_{1-x}P_x)S_5I$. a) Limiting voltage approached at long charging times (U_0); b) amplitude of the exponential growth (A_0); c) characteristic relaxation time (τ); and d) coefficient describing the voltage linear increase with time (k).

transport and relaxation processes in the superionic material. Upon $Ge^{4+} \rightarrow P^{5+}$ substitution, the characteristic relaxation time τ increases from 27 s (Ag_7GeS_5I) to 74 s (Ag_6PS_5I). This indicates slowing down of the charging processes and a stronger influence of diffusion limitations, with the maximum τ values observed for the phosphorus-containing compositions.

In addition to the exponential relaxation component, the voltage–time dependences $U(t)$ of the electrochemical cells during charging contain a linear contribution characterized by the coefficient k. The parameter k reflects slow processes that lead to a gradual increase in the voltage with time even after the fast diffusion relaxation is completed [29, 30]. It describes slow accumulation of polarization caused by the defect structure of the electrolyte (grain boundaries, pores, surfaces) as well as transport bottlenecks in the crystal lattice [29, 30]. Defects and interfaces significantly affect the rate of ionic transport through the material. Structural inhomogeneities result in potential jumps and a slow voltage rise under constant current. The parameter k is associated with (i) polarization build-up at the phase interfaces (Ag|SE and SE|Se) arising from limited ionic conductivity and slow interfacial reconstruction; (ii) diffusion limitations in the bulk electrolyte, where establishment of an equilibrium distribution of Ag^+ ions requires long times; and (iii) irreversible processes such as formation or decomposition of Ag_2Se phase inclusions at the interface, which manifest themselves by a quasi-linear voltage variation.

Analysis of the composition dependence of the parameter k shows that its maximum value is reached for the mixed composition $Ag_{6.5}P_{0.5}Ge_{0.5}S_5I$ (Ge:P = 1:1), whereas it remains at the level of 10^{-5} V/s for the end-member Ge- and P-rich compositions. Such a nonlinear dependence suggests that the structural features of the crystal lattice and the distribution of defects in the solid electrolyte play a key role in the slow charge accumulation processes [29]. For compositions with partial Ge → P substitution (x = 0.5), formation of a highly disordered structure with a maximized number of defects and vacancies available for Ag^+ ion migration is likely. This leads to enhanced polarization processes and an increased contribution of the linear component. In contrast, in Ge-rich and P-rich compositions, the structure is more ordered, which reduces the possibility of long-term polarization build-up and results in smaller k values [31]. Hence, the parameter k may be considered as a marker of irreversible and slow charge redistribution processes, sensitive to the composition and defect structure of the superionic electrolyte. Its concentration dependence reflects the balance between the ion mobility, structural disorder, and interfacial reactions, which together define the efficiency of operation of the electrochemical cell.

For analysis of the $U(t)$ dependences during charging of the $Ag|Ag_{7-x}(Ge_{1-x}P_x)S_5I|Se$ cells, we used an approach based on determining the characteristic relaxation time τ, which defines the rate of establishing an equilibrium distribution of ions during charging and is related to the diffusion time of Ag^+ ions through the electrolyte. In the approximation of one-dimensional diffusion across the disk thickness L, the diffusion coefficient D of the ions is given by the following expression [29]:

$$D = \frac{L^2}{\pi^2 \tau}. \tag{6}$$

The relationship between the diffusion coefficient D, ion mobility μ, concentration of mobile ions n and ionic conductivity σ_i is described by the Nernst–Einstein relation [30]:

$$\mu = \frac{Dq}{k_B T},\ \sigma_i = nq\mu = nq^2 \frac{D}{k_B T},\ n = \frac{\sigma_i k_B T}{q^2 D}, \tag{7}$$

where q is the ionic charge ($q = e = 1.6 \cdot 10^{-19}$ C for Ag^+), k_B is the Boltzmann constant, and T is the absolute temperature respectively. The ionic resistance of the cell is determined by the following geometrical relation:

$$R_{ion} = \frac{L}{\sigma_i A}, \tag{8}$$

where $A = \pi d^2/4$ is the electrode area and d is the diameter of the superionic disk respectively.

The corresponding effective capacitance C of the cell within the RC approximation may be found as

$$C = \frac{\tau}{R}. \tag{9}$$

In presence of an electronic contribution to the conductivity, the transference number, characterizing the fraction of the current carried by ions, was determined as [31]

$$t_{ion} = \frac{\sigma_i}{\sigma_i - \sigma_e}, \tag{10}$$

where σ_i and σ_e are the ionic and electronic components of the conductivity, respectively.

Table 2. Electrolyte parameters calculated from the experimental values of τ, σ_i, and σ_e [13]. (Assumptions: one-dimensional diffusion across a disk thickness L = 1 mm; temperature T = 298 K; *RC* model used as an approximation for the effective capacitance.)

	Chemical composition	τ, s	σ_i, S/cm	$\sigma_e \cdot 10^{-7}$, S/cm	$D \cdot 10^{-9}$, m^2/s	n, 10^{24}, m^{-3}	$\mu \cdot 10^{-8}$, $m^2/(V \cdot s)$	R_{ion}, Ohm	C, F	t_{ion}
1	Ag_7GeS_5I	27.1	0.0223	≈11	3.73	5.97	14.5	91.6	0.30	0.9993
2	$Ag_{6.75}P_{0.25}Ge_{0.75}S_5I$	32.6	0.0476	≈2	3.11	5.21	12.1	126.1	0.26	0.9970
3	$Ag_{6.5}P_{0.5}Ge_{0.5}S_5I$	40.4	0.0346	≈0.01	2.51	5.82	9.8	139.9	0.29	0.9978
4	$Ag_{6.25}P_{0.75}Ge_{0.25}S_5I$	67.7	0.0118	≈15	1.50	8.25	5.8	165.4	0.41	0.9961
5	Ag_6PS_5I	74.1	0.0004	≈18	1.37	8.09	5.3	184.5	0.40	0.9942

Table 3. Approximation parameters of the charging curves $U(t)$ of the cell based on $Ag_{6.5}P_{0.5}Ge_{0.5}S_5I$ ceramics over five charge-discharge cycles.

Cycle		U_0, V	A_0, V	τ, s	k, V/s	b, V
1	$Ag_{6.5}P_{0.5}Ge_{0.5}S_5I$	0.249	0.034	113.5	$4.5 \cdot 10^{-5}$	0.249
2		0.269	0.133	47.7	$4.2 \cdot 10^{-5}$	0.269
3		0.285	0.141	43.8	$4.6 \cdot 10^{-5}$	0.223
4		0.296	0.154	38.7	$8.2 \cdot 10^{-5}$	0.124
5		0.317	0.168	40.4	$15.5 \cdot 10^{-5}$	0.318

Table 2 presents the results of the calculations of the diffusion coefficient D, concentration of mobile ions n, mobility μ, ionic resistance R_{ion}, effective capacitance C, and transference number t_{ion} for five compositions of $Ag|Ag_{7-x}(Ge_{1-x}P_x)S_5I|Se$.

It can be seen from Tables 1 and 2 that there is a correlation between the increase in the phosphorus concentration and the growth of U_0 and τ as well as the decrease in A_0. The maximum value of the parameter k for the composition $Ag_{6.5}P_{0.5}Ge_{0.5}S_5I$ (Ge/P = 1) indicates an enhanced polarization contribution, which may be explained by non-equilibrium processes at the phase boundaries. These parameters also vary at increasing the number of charge-discharge cycles. The most pronounced changes in the $U(t)$ dependences are observed for the $Ag_{6.5}P_{0.5}Ge_{0.5}S_5I$ composition (Fig. 5). Table 3 and Fig. 8 present the approximation parameters of the charging curves $U(t)$ for the cell based on the $Ag_{6.5}P_{0.5}Ge_{0.5}S_5I$ ceramics over five charge-discharge cycles. As can be seen from Fig. 8, the variation of the parameters for this composition becomes quite significant at increasing the cycle number.

The increase in the limiting voltage U_0 from 0.249 V (1st cycle) to 0.317 V (5th cycle) indicates a rise in the steady-state electromotive force of the cell during prolonged charging. This reflects changes in the distribution of the chemical potentials of Ag, stabilization of the interfacial layers, and accumulation of ionic charge, which together lead to an increase in the final potential.

The growth of the amplitude A_0 of the exponential component from 0.034 to 0.168 V means that contribution of the fast relaxation stage to formation of the total voltage becomes more significant in the subsequent cycles. After the initial "formative" charging cycle, fast transport processes become more pronounced, resulting in "optimization" of the ionic pathways.

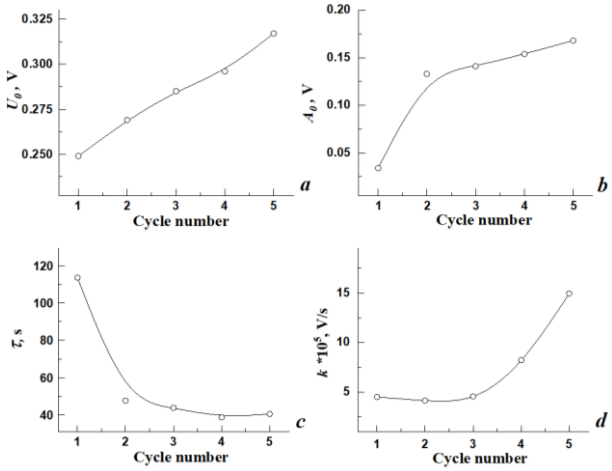

Fig. 8. Variation of approximation parameters of charging curves $U(t)$ for the $Ag_{6.5}P_{0.5}Ge_{0.5}S_5I$ ceramic cell over five charge-discharge cycles. a) Limiting voltage approached at long charging times (U_0); b) amplitude of the exponential growth (A_0); c) characteristic relaxation time (τ); and d) coefficient describing the linear voltage increase with time (k).

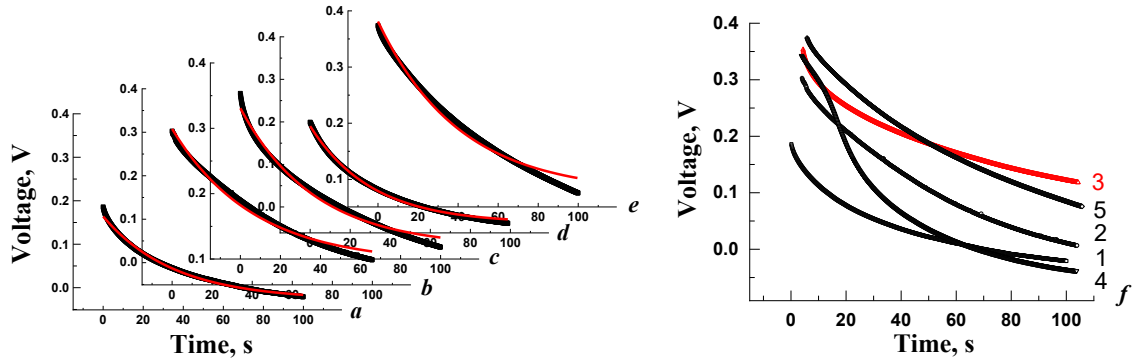

Fig. 9. Results of approximation of the discharge curves by exponential dependences. a) Ag_7GeS_5I, b) $Ag_{6.75}P_{0.25}Ge_{0.75}S_5I$, c) $Ag_{6.5}P_{0.5}Ge_{0.5}S_5I$, d) $Ag_{6.25}P_{0.75}Ge_{0.25}S_5I$, e) $Ag_6P_5S_5I$, and f) discharge curves for the cells for the fifth cycle: Ag_7GeS_5I (1), $Ag_{6.75}P_{0.25}Ge_{0.75}S_5I$ (2), $Ag_{6.5}P_{0.5}Ge_{0.5}S_5I$ (3), $Ag_{6.25}P_{0.75}Ge_{0.25}S_5I$ (4), and $Ag_6P_5S_5I$ (5).

The decrease in the relaxation time τ from 113.5 s (1st cycle) to ~39–40 s in the 4th–5th cycles reflects acceleration of establishing the ionic distribution profile during charging, i.e., enhancement of effective diffusion of Ag^+ ions within the electrolyte. This behavior is typical for "running-in" processes, during which local barriers to ion transport (poor contacts, blocking defects) are eliminated, the electrode–electrolyte contact improves, and more stable ionic channels are formed [32, 33].

The increase in the linear component k from $4.5\cdot10^{-5}$ V/s (1st cycle) to $15.5\cdot10^{-5}$ V/s (5th cycle) points to strengthening of slow irreversible or quasi-stable processes in $Ag_{6.5}P_{0.5}Ge_{0.5}S_5I$. Such processes may include polarization buildup at phase boundaries, slow phase transformations (formation and growth of Ag_2Se inclusions), and relaxation of space-charge layers. The increase in k in the later cycles indicates intensification of these slow processes despite the acceleration of the diffusion stage (reduction of τ). This may be caused by progressive irreversible interfacial changes as well as phase redistributions under repeated cycling.

The non-monotonic dynamics of the parameter b may be attributed to variations in the initial polarization prior to start of each measurement cycle. This parameter reflects the changes in the initial state of the linear component of $U(t)$ and may be associated with differences in the initial degree of interface saturation, changes in contacts, or local phase transformations occurring during the preceding cycle.

3.4. Discharge process

Compared to charging, the discharge process of electrochemical cells proceeds more intensely. Fig. 9 shows the dependences $U(t)$ for the cells during discharge (fifth cycle) under a constant discharge current of 1 mA for 100 s. As can be seen from Fig. 9, the $U(t)$ curves exhibit an exponential behavior. These curves were approximated by the following expression:

$$U_d(t) = \left(U_{0d} - A_{0d} e^{-\frac{t}{\tau_d}} \right), \qquad (11)$$

where the parameters U_{0d}, A_{0d} and τ_d have the same physical meaning as in the charging process. The subscript "*d*" denotes the discharge process of the cell. The results of the approximation of the discharge curves $U(t)$ are summarized in Table 4.

It can be seen from Table 4 that the limiting voltage U_{0d} varies from negative values (–0.038 V for $Ag_{6.25}P_{0.75}Ge_{0.25}S_5I$) to positive ones (0.118 V for $Ag_{6.5}P_{0.5}Ge_{0.5}S_5I$) during discharge. Positive U_{0d} values reflect presence of residual polarization and an incompletely discharged capacity. A fraction of Ag^+ ions remains trapped in metastable states, forming a "residual charge". Negative U_{0d} values indicate overdischarge and cell overvoltage: the cell discharges below zero potential, which may be associated with a reversible transition-decomposition of Ag_2Se, or with asymmetry between the charging and discharging processes.

The amplitude of the exponential component A_{0d} lies within the range 0.19…0.31 V. The higher the A_{0d}, the larger the fraction of accumulated charge released during the initial stage of discharge. The maximum A_{0d} values were recorded for $Ag_{6.75}P_{0.25}Ge_{0.75}S_5I$ and Ag_6PS_5I (~0.31 V), indicating their enhanced charge storage capability. The minimum A_{0d} (0.192 V) observed for Ag_7GeS_5I suggests a lower capacitive response.

The parameter τd describes the rate of voltage decay during the discharge process. Prolonged discharge ($\tau_d \approx 40$ s) is observed for $Ag_{6.75}P_{0.25}Ge_{0.75}S_5I$ and Ag_6PS_5I, which indicates a slower "release" of ions and a more stable capacitive behavior. In contrast, the short $\tau_d = 26.4$ s in $Ag_{6.25}P_{0.75}Ge_{0.25}S_5I$ points to a rapid voltage drop and lower stability of the accumulated charge.

During discharge, an electrochemical cell releases the stored charge due to reverse motion of Ag^+ ions from the selenium film through the superionic electrolyte. The exponential nature of the voltage decay ($Ae^{-t/\tau}$) reflects relaxation of the space-charge regions and reduction of polarization at the electrode–electrolyte interfaces. The value of τ_d is related to the effective diffusion coefficient of Ag^+: larger τd correspond to slower diffusion and a more "extended" discharge, whereas smaller τ_d correspond to a faster voltage decay.

The residual potential U_{0d} and its sign indicate that the discharging is not completely fully symmetrical with respect to the charging because the accumulated interfacial processes (formation/decomposition of Ag_2Se and charge accumulation at the phase boundary) shift the equilibrium potential.

Therefore, the discharge efficiency is defined by a combination of three parameters: U_{0d}, A_{0d}, and τ_d. The most stable discharge characteristics were exhibited by $Ag_{6.75}P_{0.25}Ge_{0.75}S_5I$ and Ag_6PS_5I, where as $Ag_{6.25}P_{0.75}Ge_{0.25}S_5I$ demonstrated a faster and less efficient discharge.

Analysis of the approximation parameters of the $U(t)$ curves for the fifth cycle (Table 1 − charging, Table 4 − discharging) reveals noticeable differences in the mechanisms of charge accumulation and release in $Ag_{7-x}(Ge_{1-x}P_x)S_5I$-based cells.

Limiting voltage. During charging, the limiting voltage U_0 gradually increases from 0.212 V (Ag_7GeS_5I) to 0.405 V (Ag_6PS_5I), reflecting an increase in the stored charge and contribution of polarization processes. In contrast, during discharging, the residual voltages are much lower (0…0.12 V) or even negative. This asymmetry indicates that charging results in higher potential accumulation than can be recovered during discharge, which points to hysteresis and partial energy loss due to slow and irreversible processes.

Exponential amplitude. For charging, the amplitudes of the exponential component are relatively small (0.055…0.236 V) and decrease upon moving from Ge-rich to P-rich compositions. During discharging, however, these amplitudes are higher (0.19…0.31 V), indicating a more "rapid" release of the accumulated charge. Hence, the charge accumulation proceeds slower and partly linearly, while the release occurs predominantly through the exponential mechanism.

Relaxation time. For charging, the relaxation time increases from 27 to 74 s, reflecting a slowdown in formation of potential at increasing the phosphorus content. For discharging, the relaxation times remain within the interval 26…41 s, *i.e.* lower than during charging. This confirms that charge release proceeds faster than charge accumulation and is less limited by structural effects.

Linear component. The linear contribution is observed only during charging (up to $15.5 \cdot 10^{-5}$ V/s for $Ag_{6.5}P_{0.5}Ge_{0.5}S_5I$). During discharging, no linear contribution is detected. Therefore, slow processes (polarization, Ag_2Se phase formation, space-charge accumulation) manifest themselves predominantly during charging, whereas release of the charge during discharging is governed by the fast exponential mechanism.

Comparison of the data shows that charging and discharging are not mirror-symmetric processes. Charging of the cells is a multicomponent process that includes fast exponential relaxation and slow linear voltage increase caused by interfacial polarization buildup and structural rearrangements (growth of Ag_2Se inclusions, formation of space charge). During charging, not only ionic charge is accumulated but also a polarization contribution associated with slow structural modifications and interfacial reactions. This is reflected by the high U_0 values and presence of the linear contribution k.

In contrast, the discharge process is described by a pure exponential dependence, reflecting the relaxation of Ag^+ ions and release of polarization. Its mechanism is "cleaner", and this process is accompanied by fewer irreversible effects, although negative residual voltages may appear under strong interfacial interactions. The discharge is dominated by the exponential voltage decay, characterized by shorter relaxation times and smaller final values of U_{0d}, which indicates partial loss of the accumulated charge and presence of hysteresis between the forward and reverse processes.

The hysteresis (asymmetry) between charging and discharging confirms that charge accumulation and release are not mirror processes. This is related to the asymmetry of interfacial reactions, unequal contributions of defect structures, and different conditions for stabilization/decomposition of phase inclusions at the interface.

Therefore, the efficiency of the cells is limited by charge-discharge asymmetry, which arises from interfacial polarization and irreversible processes during charging. The most pronounced differences are observed in P-rich compositions, consistent with their higher tendency toward structural polarization.

3.5. Current-voltage characteristic of the Ag|SE|Se electrochemical cell

An important analytical tool for determining the predominant type of conductivity, the value of ionic resistance and the threshold activation voltage for ion transport as well as for identifying the influence of interfacial processes at the electrodes on the electrical parameters is the study of CVC of the electrochemical cell [34, 35].

Among the investigated $Ag_{7-x}(Ge_{1-x}P_x)S_5I$ heterostructures, the Ag_6PS_5I composition exhibits the highest limiting charging voltage ($U_0 \approx 0.405$ V), the longest relaxation time ($\tau \approx 74$ s), and characteristic features of charge accumulation associated with pronounced interfacial processes. For this composition, polarization effects are the most significant, while the fraction of the exponential component of charging is minimal, indicating predominance of slow diffusion limitations. Therefore, this composition is optimal for identifying the activation nature of conductivity and establishing correlations with the charging-discharging processes. Among the studied $Ag_{7-x}(Ge_{1-x}P_x)S_5I$ heterostructures, Ag_6PS_5I most clearly reveals ionic transport limitations that are critical for assessing performance of electrochemical energy devices.

For the Ag_6PS_5I composition, the CVC of the Ag|SE|Se electrochemical cell was studied using an AUTOLAB PGSTAT302N potentiostat/galvanostat. The resulting CVC for the $Ag|Ag_6PS_5I|Se$ cell presented

in Fig. 10 exhibits a symmetric nonlinear shape. At the voltages $|U| < 0.05$ V, the current is nearly absent, indicating a negligible electronic contribution to conductivity. At the positive voltages above 0.05…0.1 V, a sharp increase in the current up to a maximum value of ~$1.4 \cdot 10^{-3}$ A is observed, followed by its gradual decrease in the range of 0.3 to 0.8 V due to ion transport limitations caused by diffusion and interfacial polarization. The linear current growth up to the peak value ($1.4 \cdot 10^{-3}$ A) indicates the transport of Ag^+ ions through the electrolyte and their reduction on selenium. Ag_2Se is formed as an electron-conducting product at the interface. The peak at $U \approx 0.14$ V corresponds to the maximum rate of the electrochemical reaction prior to the onset of polarization. The subsequent decrease in the current after the peak is attributed to cathodic polarization, which slows down ion transport. A passivating phase may also form at the Se|Ag^+ interface, thereby reducing the current.

In the negative voltage region, CVC exhibits similar behavior. However, an asymmetry near zero is observed, reflecting the differences between the anodic and cathodic processes. Under reverse bias, the current is initially negative (redox transitions or product dissolution). At larger negative voltages (down to ~ –1 V), the current saturates and then returns to zero, indicating symmetric polarization and restoration of the ionic concentration balance. In the range of –0.6...0.3 V, a "mirror-like" current drop is observed, which is indicative of partial reversibility and possible capacitive nature of the current. The CVC does not coincide for the forward and reverse scans, which may be attributed to slow interfacial processes, charge accumulation, and interface rearrangement.

Under applied forward bias, Ag^+ ions migrate through the solid electrolyte. At the selenium interface, they are reduced to form Ag_2Se, which leads to an increase in the current. As Ag_2Se accumulates, the interfacial resistance increases, resulting in a current decrease. Upon reversal of the polarity, Ag^+ ions begin to move back, or reverse redox processes occur. A small capacitive contribution is also detected, which is most likely associated with charge accumulation at the interfaces.

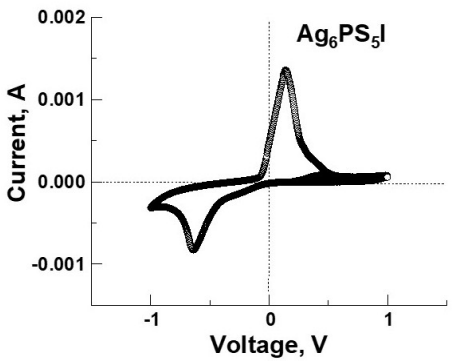

Fig. 10. Current-voltage characteristic of the Ag_6PS_5I-based cell (fifth cycle).

Comparison of the CVC with the galvanostatic "charge-discharge" curves (5th cycle) demonstrates good agreement: the limiting charging voltage ($U_0 \approx 0.405$ V), the small amplitude of the exponential component ($A_0 \approx 0.055$ V), and the increased relaxation time ($\tau \approx 74$ s) correspond to the activation and current saturation region on CVC. During discharge ($U_{0d} \approx 0.076$ V, $A_{0d} \approx 0.305$ V, $\tau_d \approx 41$ s), an exponential voltage decay is observed, which correlates with the rapid decrease of the current in the negative part of the CVC.

Linear approximation of the charging section near zero yielded a resistance value of about 200 Ohm, which is comparable with the ionic resistance ($R_{ion} \approx 185$ Ohm, Table 3) calculated from the charge-discharge curves. This confirms predominantly ionic character of the transport (ionic transference number $t_{ion} \approx 0.994$, Table 3).

Hence, comparison and joint analysis of the CVC and charge-discharge cycles make it possible to identify the characteristic features of cell operation and reveal a direct correlation between the activation onset of the ionic current and the accumulation of interfacial polarization during charging, as well as the exponential release of charge during discharging. These results confirm the consistency of the experimental methods and the adequacy of the proposed process model, as well as indicate a promise of the Ag_6PS_5I composition for application in solid-state electrochemical energy devices.

4. Conclusions

The carried out studies of the charge-discharge characteristics of heterostructures based on superionic electrolytes $Ag_{7-x}(Ge_{1-x}P_x)S_5I$ have shown that electrical properties of such heterostructures strongly depend on the electrolyte chemical composition and phosphorus concentration. This is related to changes in the number of vacancies and the degree of structural disorder in the Ag^+ cation sublattice. A pronounced asymmetry between charging and discharging has been observed. The accumulated potential exceeds the value recovered during discharge, which is associated with interfacial polarization, formation/decomposition of Ag_2Se, and irreversible processes at the electrode–electrolyte interface.

The most stable and efficient characteristics were demonstrated by the $Ag_{6.75}P_{0.25}Ge_{0.75}S_5I$ and Ag_6PS_5I compositions, while other compounds exhibited accelerated and less efficient discharge. Combined analysis of the CVC and charge-discharge cycles confirmed the adequacy of the employed process model and indicated a direct correlation between the activation of ionic current and the accumulation of interfacial polarization during charging, as well as the exponential release of charge during discharging.

Therefore, $Ag_{7-x}(Ge_{1-x}P_x)S_5I$ solid solutions represent promising materials for application in solid-state electrochemical energy devices, including sensors, batteries, and energy storage systems.

Acknowledgements

This work has been supported by the grants EU NextGenerationEU through the Recovery and Resilience Plan for Slovakia under the project No. 09I03-03-V01-00096 and the grant of the Slovak Research and Development Agency under the contract APVV-23-0049. S. Vorobiov acknowledges financial support provided under the NextGenerationEU through the Recovery and Resilience Plan for Slovakia under the project No. 09I03-03-V0400179.

References

1. Laqibi M., Cros B., Peytavin S., Ribes M. New silver superionic conductors Ag_7XY_5Z (X = Si, Ge, Sn; Y = S, Se; Z = Cl, Br, I) – synthesis and electrical properties. *Solid State Ionics*. 1987. **23**. P. 21. https://doi.org/10.1016/0167-2738(87)90077-4.
2. Hull S. Superionics: Crystal structures and conduction processes. *Rep. Prog. Phys*. 2004. **67**. P. 1233–1314. https://doi.org/10.1088/0034-4885/67/7/R05.
3. Agrawal R.C., Gupta R.K. Superionic solid: composite electrolyte phase – an overview. *J. Mater. Sci*. 1999. **34**. P. 1131–1162. https://doi.org/10.1023/A:1004598902146.
4. Kraft M.A., Ohno S., Zinkevich T. *et al*. Inducing high ionic conductivity in the lithium superionic argyrodites $Li_{6+x}P_{1-x}Ge_xS_5I$ for all-solid-state batteries. *J. Am. Chem. Soc.* 2018. **140**, No 47. P. 16330–16339. https://doi.org/10.1021/jacs.8b10282.
5. Pogodin A.I., Filep M.J., Izai V.Yu. *et al*. Crystal growth and electrical conductivity of Ag_7PS_6 and Ag_8GeS_6 argyrodites. *J. Phys. Chem. Solids.* 2022. **168**. P. 110828. https://doi.org/10.1016/j.jpcs.2022. 110828.
6. Yamamoto O. Solid state ionics: a Japan perspective. *Sci. Technol. Adv. Mater.* 2017. **18**, No 1. P. 504–527. https://doi.org/10.1080/14686996. 2017.1328955.
7. Kuhs W.F., Nitsche R., Scheunemann K. The argyrodites – A new family of the tetrahedrally close-packed structures. *Mater. Res. Bull*. 1979. **14**, No 2. P. 241–248. https://doi.org/10.1016/0025-5408(79)90125-9.
8. Studenyak I.P., Pogodin A.I., Filep M.J. *et al*. Influence of heterovalent cationic substitution on electrical properties of $Ag_{6+x}(P_{1-x}Ge_x)S_5I$ solid solutions. *J. Alloys Compd.* 2021. **873.** P. 159784. https://doi.org/10.1016/j.jallcom.2021.159784.
9. Pogodin A., Filep M., Malakhovska T. *et al*. Microstructural, mechanical properties and electrical conductivity of $Ag_7(Si_{1-x}Ge_x)S_5I$-based ceramics. *Ionics.* 2024. **30**. P. 3339–3356. https://doi.org/10.1007/s11581-024-05513-5.
10. Belin R., Zerouale A., Pradel A., Ribes M. Ion dynamics in the argyrodite compound Ag_7GeSe_5I: non-Arrhenius behavior and complete conductivity spectra. *Solid State Ionics*. 2001. **143**, Nos 3–4. P. 445–455. https://doi.org/10.1016/S0167-2738(01)00883-9.
11. Evain M., Gaudin E., Boucher F. *et al*. Structures and phase transitions of the Ag_7PSe_6 (A = Ag, Cu) argyrodite-type ionic conductors. I. Ag_7PSe_6. *Acta Crystallogr. B*. 1998. **54**. P. 376–383. https://doi.org/10.1107/ S0108768197019654.
12. Pogodin A.I., Filep M.J., Malakhovska T.O. *et al*. Microstructural, mechanical and electrical properties of superionic $Ag_{6+x}(P_{1-x}Ge_x)S_5I$ ceramic materials. *J. Phys. Chem. Solids*. 2022. **171**. P. 111042. https://doi.org/10.1016/j.jpcs.2022. 111042.
13. Pogodin A., Filep M., Malakhovska T. *et al*. Recrystallization and heterovalent substitution effects on mechanical and electrical parameters of $Ag_{6+x}(P_{1-x}Ge_x)S_5I$-based ceramics. *J. Eur. Ceram. Soc.* 2024. **44**, No 6. P. 4097–4110. https://doi.org/10.1016/j.jeurceramsoc.2023.12.093.
14. Pogodin A., Filep M., Malakhovska T. *et al*. Influence of recrystallization process on ionic conductivity of $Ag_{6.75}P_{0.25}Ge_{0.75}S_5I$ based ceramic materials. *Ceram. Int*. 2023. **49**, No 21. P. 33764–33772. https://doi.org/10.1016/j.ceramint.2023.08.068.
15. Pang B., Gan Y., Xia Y. *et al*. Regulation of the interfaces between argyrodite solid electrolytes and lithium metal anode. *Front. Chem*. 2022. **10**. P. 837978. https://doi.org/10.3389/fchem.2022.837978.
16. Zhang Z., Suna Y., Duan X. *et al*. Design and synthesis of room temperature stable Li-argyrodite superionic conductors via cation doping. *J. Mater. Chem. A*. 2019. **7**. P. 2717–2722. https://doi.org/10.1039/C8TA10790D.
17. Feng D., Taskinen P., Tesfaye F. Thermodynamic stability of Ag_2Se from 350 to 500 K by a solid state galvanic cell. *Solid State Ionics.* 2013. **231**. P. 1–4. https://doi.org/10.1016/j.ssi.2012.10.013.
18. Zerouale A., Cros B., Deroide B., Ribes M. Electrical properties of Ag_7GeSe_5I. *Solid State Ionics.* 1988. **28–30**. Part 2. P. 1317–1319. https://doi.org/10.1016/0167-2738(88)90378-5.
19. Oehsen U.V., Schmalzried H. Thermodynamic investigations of Ag_2Se. *Ber. Bunsenges. Phys. Chem.* 1981. **85**. P. 7–14. https://doi.org/10.1002/bbpc.
20. Kogai V.Y. Reaction-diffusion-induced explosive crystallization in a metal–selenium nanometer film structure. *Techn. Phys.* 2016. **61**, No 3. P. 461–463. https://doi.org/10.1134/S1063784216030117.
21. Johnson D.B., Brown L.C. Lateral diffusion in Ag–Se thin-film couples. *J. Appl. Phys.* 1969. **40**, No 1. P. 149–152. https://doi.org/10.1063/1.1657020.
22. Pogodin A.I., Filep M.J., Kokhan O.P. *et al*. Peculiarities of single crystal growth of solid solution in systems Ag_6PS_5I–Ag_7GeS_5I and Ag_7SiS_5I–Ag_7GeS_5I. *Sci. Bull. Uzhh. Univ. Ser. Chem.* 2021. **45**, No 1. P. 29–34. https://doi.org/10.24144/2414-0260.2021.1.29-34.
23. Malakhovska T.O., Pogodin A.I., Filep M.J. *et al*. Preparation and properties of ceramic materials in the Ag_6PS_5I–Ag_7GeS_5I system. *Sci. Bull. Uzhh. Univ. Ser. Chem.* 2023. **48**, No 2. P. 16–22. https://doi.org/10.24144/2414-0260.2022.2.16-22.

24. Belin R., Aldon L., Zerouale A. *et al*. ChemInform abstract: Crystal structure of the non-stoichiometric argyrodite compound $Ag_{7-x}GeSe_5I_{1-x}$ (x = 0.31). A highly disordered silver superionic conducting material. *ChemInform.* 2001. **32**, No 31. P. 251–265. https://doi.org/10.1002/chin.200131024.
25. Saito Y., Sato M., Shiojiri M. Orientation in Ag_2Se polymorphic films produced by the reaction of silver films with selenium. *Thin Solid Films*. 1981. **79**, No 3. P. 257–266. http://doi.org/10.1016/0040-6090(81)90314-X.
26. Bernede J.C., Conan A., Fouesnant E. *et al*. Polarized memory switching effects in Ag_2Se/Se/M thin film sandwiches. *Thin Solid Films*. 1982. **97**. P. 165–171. https://doi.org/10.1016/0040-6090(82)90225-5.
27. Sun F., Li Y., Wu Z. *et al*. *In situ* reactive coating of metallic and selenophilic Ag_2Se on Se/C cathode materials for high performance Li–Se batteries. *RSC Adv*. 2018. **8**. P. 32808–32813. https://doi.org/10.1039/c8ra06484a.
28. Li D.P., Zheng Z., Shui Z.Y. *et al*. Using elemental Se and Ag to grow pure Ag_2Se dendrites/dendritic-films of highly oriented (001) nanocrystals. *J. Phys. Chem. C*. 2008. **112**, No 8. P. 2845–2850. https://doi.org/10.1021/jp710190j.
29. Shah D.B., Nguyen H.Q., Grundy L.S. *et al*. Difference between approximate and rigorously measured transference numbers in fluorinated electrolytes. *Phys. Chem. Chem. Phys.* 2019. **21**. P. 7857–7866. https://doi.org/10.1039/C9CP00216B.
30. Bard A.J., Faulkner L.R., White H.S. *Electrochemical Methods: Fundamentals and Applications*. 3nd ed. John Wiley & Sons, 2022.
31. Fong K.D., Self J., Diederichsen K.M. *et al.* Ion transport and the true transference number in nonaqueous polyelectrolyte solutions for lithium ion batteries. *ACS Cent. Sci*. 2019. **5**, No 7. P. 1250–1260. https://doi.org/10.1021/acscentsci.9b00406.
32. Zhang S., Li Y., Bannenberg L.J. *et al*. The lasting impact of formation cycling on the Li-ion kinetics between SEI and the Li-metal anode and its correlation with efficiency. *Sci. Adv*. 2024. **10**, No 3. P. eadj8889. https://doi.org/10.1126/sciadv.adj8889.
33. Alsaç E.P., Nelson D.L., Yoon S.G. *et al*. Characterizing electrode materials and interfaces in solid-state batteries. *Chem. Rev*. 2025. **125**. P. 2009–2119. https://doi.org/10.1021/acs.chemrev.4c00584.
34. Nie K., Hong Y., Qiu J. *et al*. Interfaces between cathode and electrolyte in solid state lithium batteries: Challenges and perspectives. *Front. Chem*. 2018. **6**. P. 1–19. https://doi.org/10.3389/fchem.2018.00616.
35. Sudharma J.M., Jayaprakash S.K., Suriyakumar S. *et al*. Carbon spheres with catalytic silver centres as selenium hosts for stable lithium–selenium batteries. *Energy Adv*. 2024. **3**. P. 215–223. https://doi.org/10.1039/D3YA00487B.

Authors and CV

Vitaliy S. Bilanych, Assoc. Prof., CSc., Head of the Department of Applied Physics and Quantum Electronics, Uzhhorod National University. Authored over 90 publications and 4 patents. Areas of professional interest: study of nanostructuring and charge redistribution in chalcogenide films under electron and laser irradiation; charge–discharge processes and ion transport in solid-state cells based on superionic and chalcogenide materials; internal friction and relaxation in chalcogenide glasses; development of gas sensors using nanostructured oxides (SnO_2, In_2O_3) with Au/Pt nanoparticles.
https://orcid.org/0000-0003-4293-5675

Anatoliy A. Slyvka, PhD student, Department of Applied Physics and Quantum Electronics, Uzhhorod National University. He is the author of 2 publications. The area of his scientific interests includes electron-photon emission from the surfaces of alkali halide crystals modified with metal nano-particles and ion transport processes in superionic conductors with argyrodite-type structure.
E-mail: anatolii.slyvka@uzhnu.edu.ua,
https://orcid.org/0000-0002-9173-731X

Serhii I. Vorobiov, defended his PhD in Physics and Mathematics in 2015 at the Sumy State University, Ukraine. Postdoctoral researcher at the Institute of Physics, Faculty of Science, P.J. Safarik University, Slovakia. He is the author of 78 publications indexed in Scopus and Web of Science databases and 1 patent. The area of his scientific interests includes nanofabrication and thin film technology, and magnetic and magnetoresistance properties of nano and mesoscopic systems.
E-mail: serhii.vorobiov@upjs.sk,
https://orcid.org/0000-0002-5884-3292

Ihor M. Mohylyuk, received a M.Sc degree in applied physics and nanomaterials at the Uzhhorod National University, currently he is an Engineer of the Department of Applied Physics and Quantum Electronics at the same university. Research interests: gas-sensitive materials based on tin dioxide, superionic conductors.
E-mail:ihormohyliyk@gmail.com,
https://orcid.org/0009-0009-3871-0001

Artem I. Pogodin, PhD in Inorganic Chemistry (2016), Senior Researcher at the Uzhhorod National University. Authored over 100 articles and 100 patents. The area of his scientific interests includes solid state chemistry, crystal growth, and materials science.
E-mail: artempogodin88@gmail.com,
https://orcid.org/0000-0002-2430-3220

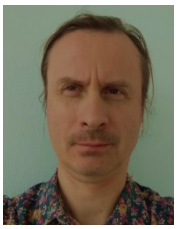

Vladimir Komanicky, defended his PhD thesis in Chemistry in 2003 at the University of California. Leading Scientist in the Electrocatalysis and Nanotechnology group at the Institute of Physics of the P.J. Safarik University in Kosice. Author of 141 publications, 2 patents and 2 textbooks. The area of his scientific interests includes nanotechnology, electrocatalysis, semiconductor physics, magnetism and superconductivity.
E-mail: vladimir.komanicky@upjs.sk,
https://orcid.org/0000-0001-8649-1987

Tetyana O. Malakhovska, PhD in Inorganic Chemistry (2010), Senior Researcher at the Uzhhorod National University. Authored 70 articles and 10 patents. The area of her scientific interests includes solid state chemistry and materials science.
E-mail: t.malakhovska@gmail.com,
https://orcid.org/0000-0001-7309-4894

Authors' contributions

Bilanych V.S.: conceptualization, methodology, validation, supervision, writing – original draft.
Slyvka A.A.: investigation, validation, data curation.
Vorobiov S.I.: methodology, supervision, investigation, validation.
Pogodin A.I.: conceptualization, methodology, resources.
Malakhovska T.O.: methodology, formal analysis, data analysis, validation, investigation, formal analysis.
Mohylyuk I.M.: data analysis, investigation.
Komanicky V.: conceptualization, methodology, formal analysis, validation, writing – review & editing.

Зарядно-розрядні процеси у твердотільних електролітних гетероструктурах $Ag_{7-x}(Ge_{1-x}P_x)S_5I$ для електрохімічних енергетичних пристроїв

В.С. Біланич, А.А. Сливка, С.І. Воробйов, А.І. Погодін, Т.О. Малаховська, І.М. Могилюк, V. Komanicky

Анотація. У твердотільних електролітних гетероструктурах $Ag|Ag_{7-x}(Ge_{1-x}P_x)S_5I|Se$ з різним співвідношенням Ge/P були досліджені зарядно-розрядні процеси. Показано, що гетеровалентне заміщення Ge^{4+} на P^{5+} у структурі аргіродиту суттєво впливає на іонну провідність, час релаксації та поляризаційні ефекти на межі електрод–електроліт. За допомогою гальваностатичного циклування та вимірювання вольт-амперних характеристик установлено залежності параметрів $U(t)$ від складу та номера циклу. Визначено коефіцієнти дифузії, рухливість іонів Ag^+, іонний опір та числа переносу, що підтверджує переважно іонний характер переносу заряду ($t_{ion} \approx 0.994…0.999$). Порівняння кривих зарядки та розрядки виявило асиметрію процесів накопичення та вивільнення заряду, пов'язану з утворенням і розкладанням фази Ag_2Se, а також із міжфазною поляризацією. Отримані результати свідчать про високу іонну провідність і стабільність складів із частковим заміщенням Ge на P, що вказує на перспективність гетероструктур $Ag_{7-x}(Ge_{1-x}P_x)S_5I$ для застосування у твердотільних електрохімічних пристроях.

Ключові слова: суперіонні провідники, структура аргіродиту, $Ag_{7-x}(Ge_{1-x}P_x)S_5I$, твердотільні електролітні гетероструктури, дифузія іонів Ag^+, зарядно-розрядні процеси, міжфазна поляризація, твердотільні електрохімічні пристрої.